Seismoacoustic Monitoring of a Longwall Face Using Distributed Acoustic Sensing

Derrick Chambers*[1] and Jeffrey Shragge[2]

ABSTRACT

Violent, dynamic failures of rockmasses in underground mines pose significant hazards to workers and operations. Over the past several decades, hardrock mines have widely adopted seismic monitoring to help address such risks. However, coal mines, particularly those employing the longwall mining method, have struggled to implement similar monitoring strategies. This is because typical longwall mines are much larger and mine more rapidly than hardrock mines. Moreover, regulations place significant restrictions on the subsurface use of electronics in coal mines due to potentially explosive atmospheres. We present a new monitoring concept that uses distributed acoustic sensing (DAS) to turn an entire longwall face into a seismoacoustic array. After exploring the acoustic response of our sensors in the laboratory, we deployed the array at an active underground longwall mine for several days. We examine 33 events recorded by both the in-mine DAS array and a surface seismic network. We observed that the array records both seismic vibrations traveling through rock and mining equipment as well as sound waves propagating in the workings. We show that waveform moveouts are clearly visible, and that the standard deviation of the audio recordings is a straightforward yet promising metric that could help quantify burst damage. Although improvements are needed before mines can routinely use this monitoring strategy, DAS-based seismoacoustic arrays may assist in understanding coal-burst mechanisms and managing associated risks in underground longwall mines as well as enable better understanding of damage associated with dynamic failures in other underground environments.

KEY POINTS

- Underground longwall mines struggle to implement seismic monitoring that can help address dynamic failures.
- We developed a distributed acoustic sensing (DAS)-based seismoacoustic monitoring method that is well suited for longwall mines.
- The DAS-seismoacoustic array may be useful in other underground settings and for studying damage mechanics.

INTRODUCTION

Coal bursts are violent, dynamic failures occurring in underground coal mines. Similar to rockbursts experienced by hardrock mines, coal bursts can disrupt mine operations, damage equipment, and potentially result in injuries or fatalities. Although notoriously difficult to predict, Mark (2016) identified several coal burst "risk factors" that include: significant depth of cover (>450 m), dipping stratigraphy, and the presence of stiff competent rocks in the roof and/or floor. It is difficult to estimate the global impact of coal bursts, because terminology and reporting criteria vary widely between countries, but Mark (2018) identified approximately 280 coal bursts between 1983 and 2017 in the U.S. mines, seven of which resulted in one or more fatalities. In China, 200 coal mines have reported coal bursts that resulted in at least 100 fatalities and 1000 injuries in the past decade (Rong *et al.*, 2022). Likewise, the Upper Silesian Coal basin shared between Poland and the Czech Republic has experienced over 100 "significant events," some of which resulted in injuries and fatalities (Mutke *et al.*, 2015). Many other countries with coal mines have reported coal bursts, including Germany, Japan, Australia, and Russia.

Seismic monitoring is an important part of rockburst risk management in deep hardrock mines (Mendecki *et al.*, 2010). Hardrock mines primarily employ networks of accelerometers or geophones installed in boreholes drilled from mine workings. Coal mining operations, though, have struggled to adopt this type of seismic monitoring (for more than short-term

1. National Institute for Occupational Safety and Health, Spokane, Washington, U.S.A., https://orcid.org/0000-0003-3656-6607 (DC); 2. Center for Wave Phenomena and Department of Geophysics, Colorado School of Mines, Golden, Colorado, U.S.A., https://orcid.org/0000-0002-1986-0399 (JS)

*Corresponding author: derchambers@cdc.gov

Cite this article as Chambers, D., and J. Shragge (2023). Seismoacoustic Monitoring of a Longwall Face Using Distributed Acoustic Sensing, *Bull. Seismol. Soc. Am.* **XX**, 1–12, doi: 10.1785/0120220219

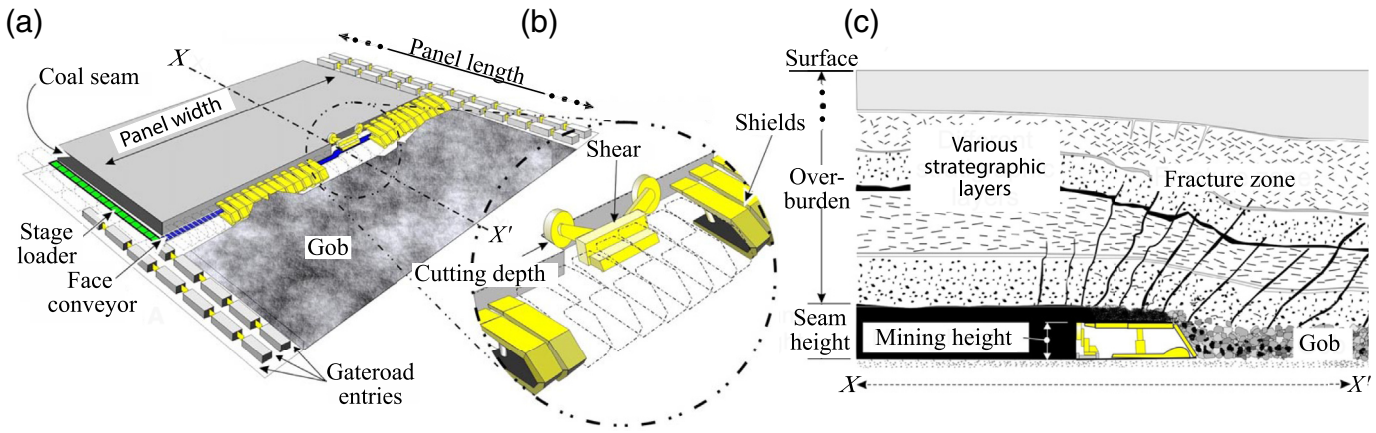

Figure 1. (a) Conceptual drawing showing an oblique view of an operating longwall, (b) a zoomed-in window of the shear, and (c) a cross section with overburden interactions. The dotted lines indicate that the arrows extend beyond the shown extents. The figure is not to scale and is modified from Karacan (2008). The color version of this figure is available only in the electronic edition.

research projects) due to vast differences in mining rates and scales, regulations governing the operation and placement of electronics, geological complexities, and a variety of other challenges (Swanson *et al.*, 2016). The greatest adoption rates are in the burst-prone Chinese coal mines where regulations mandate the implementation of "monitoring and forewarning" plans (Qi *et al.*, 2015). The scarcity of voluntary (i.e., not government mandated) adoption among many burst-prone coal mines indicates that improvements to monitoring strategies and technologies are needed for coal mines to fully realize the benefits of seismic monitoring.

The most productive form of underground coal extraction is longwall mining. Longwalls mine a block of coal called a panel, for which access tunnels are developed beforehand via continuous mining machines. Typical longwall panel widths vary from 0.1 to 0.3 km, panel lengths can reach in excess of 1.5 km, and mining rates can exceed 10 m of face advance per day. The tunnels on either side of the panel are known as gateroads. Gateroads are subdivided into entries (usually between two and five) by coal pillars left for stability. The gateroad on the side of the panel heading deeper into the mine (e.g., adjacent to the next panel to be mined) is known as the headgate, and the other is known as the tailgate. On a high level, a longwall consists of hydraulic shields for supporting the roof, an armored conveyor belt for removing the coal, and a shearer traveling up and down the face cutting and knocking the coal onto the conveyor belt (Fig. 1). Once sufficient coal is removed, groups of shields advance and the roof collapses behind them forming a caved-out zone known as a "gob" or "goaf."

Distributed acoustic sensing (DAS) is a relatively new technology that employs rapid laser pulses to sense subtle strains in fiber-optic cable (with fiber lengths of several kilometers or longer). Because DAS can use commodity fiber-optic cable approved for use anywhere in a coal mine, including the previously deployed communication fiber, DAS networks may enable entirely new or hybrid seismic monitoring approaches that are better suited for longwall mines than current monitoring methods. Although at any point along the sensing cable DAS has a much lower sensitivity than a geophone or accelerometer, its distributed nature and per-channel cost-effectiveness have made possible, or greatly improved, a wide range of geophysical sensing applications (Lindsey and Martin, 2021). DAS applications to the mining industry are rare, but a few recent studies have explored the topic. Zeng *et al.* (2021) temporarily deployed DAS cables in a few different configurations on the floor of a limestone mine to record signals from an accelerated weight-drop source and production blasts. Du Toit *et al.* (2022) monitored seismicity for two weeks with DAS at an active mine by deploying fiber along the metal mesh, which supports the mine walls, and fiber in a grouted borehole. They then compared the induced seismicity recordings to in-mine microseismic sensors. Luo and Duan (2022) used DAS with a trenched cable on the surface and a cable in a vertical borehole to monitor seismicity and caving associated with longwall coal mining.

Although the bulk of geophysical DAS research focuses on recording vibrations transmitted through solid materials, some DAS studies have recorded the transmission of mechanical waves through fluids. Zuo *et al.* (2021) characterized the signals transmitted via boat to lake-bed armored fiber cables as the first step in using ocean-bottom cables as receivers for underwater communication. Lior *et al.* (2021) used seafloor fiber cables for imaging an underwater basin using ambient noise tomography. Efforts to use fiber-optic technology to record sound waves date back at least to Cole *et al.* (1977), and several high-quality, fiber-based microphones have been commercially available for more than a decade (e.g., Bucaro *et al.*, 2005). However, efforts to use DAS, which is also known as phase-coherent optical time domain reflectometry (OTDR), to construct a distributed array of acoustic sensors is relatively

recent. Liu *et al.* (2021) demonstrated using a phase-based OTDR to create an array of 3D printed pucks wrapped with fiber for locating acoustic source located underwater and in air. Li *et al.* (2020) used a coherent OTDR to construct an array of acoustic sensors by wrapping fiber around 3D-printed hollow cylinders.

We present a new DAS-based monitoring approach, which consists of fiber-optic microphones and cable fastened to mining equipment, deployed on a longwall, for studying coal bursts occurring near the mining face. Because the seismoacoustic recordings are made in close proximity to burst damage, data of this type may provide insights about damage processes and associated hazards that are not provided by more distant recordings typical of other monitoring methods. Moreover, our approach eliminates or alleviates many of the operational challenges associated with traditional in-mine monitoring of longwall coal mines.

We begin by discussing the fabrication and testing of a DAS-based fiber-optic microphone based on the design of Li *et al.* (2020). We then detail the deployment of the seismoacoustic array on a longwall in an active underground coal mine. Next, we discuss a simple metric that shows potential for quantifying face damage and could offer insight into burst mechanics. Finally, we compare the advantages and disadvantages of this longwall DAS monitoring approach with traditional in-mine networks, discuss the potential of DAS for understanding burst damage in underground mines, and outline future work needed before routine use of fiber-optic seismoacoustic monitoring can be widely adopted by the mining industry.

ARRAY DEVELOPMENT

The seismoacoustic array consists of fiber-optic cable attached to the longwall and the DAS microphones, which we designed, fabricated, and tested in the lab. The numerical modeling efforts of Li *et al.* (2020) indicate that microphone sensitivity increases with increasing cylinder radius, decreasing wall thickness, decreasing elastic modulus (stiffness), and increasing Poisson's ratio. Rather than attempt to build a perfect microphone that optimizes all these parameters, we selected a commercially available polyethylene terephthalate glycol (PETG) cylinder typically used for packaging. PETG was preferred for its low stiffness, high Poisson's ratio, and cost-effectiveness in relation to other common plastics. Each cylinder had an outer diameter of 104.3 mm, a wall thickness of 0.7 mm, a length of 305 mm, and cost less than a few USD. We used a hand drill and custom extension to wrap approximately 90 m of single-mode, tight-buffered fiber around each cylinder to construct the microphones, which were then interconnected via single-mode signal cable approved by the Mine Safety and Health Administration (MSHA) for use in coal mines. We recorded the data presented in this article using a Treble true-phase DAS interrogator from Terra15 Pty. Ltd. The Treble interrogator is somewhat unique in that it records velocity (i.e., along-fiber deformation rate) rather than strain rate. Table 1 shows the interrogator configuration, which was identical for the lab experiment and field deployment.

TABLE 1
Distributed Acoustic Sensing Configuration

Parameter	Value
Cable length (m)	2505
Pulse length (m)	10.62
Pulse rate (Hz)	16070.97
Sample length (m)	5.72
Sample rate (Hz)	8035.5
Outgoing amplifier (mV)	165.0
Incoming amplifier (mV)	105.0

Because the performance of the DAS-microphone system depends on numerous factors, including the interrogator, cable type, cylinder geometry, and properties, we found it necessary to first evaluate the acoustic response of the system in a controlled setting. To that end, we constructed a cubic chamber, approximately 1.2 m in length, with one open side. The chamber was lined with jagged foam to dampen sound reflections. We then suspended the DAS microphone about mid-chamber and used a 12 W programmable speaker to play monotones (harmonics) ranging from 75 Hz to 2500 kHz into the chamber. We selected the lower end of this range because the speaker was incapable of producing lower frequencies, whereas the upper end represents a reasonable limit for corner frequencies of mining-induced events as small as moment magnitude −2.0 (Swanson *et al.*, 2016). We tested a measurement microphone, the MiniDSP UMIK1, in an identical manner to compare the DAS microphone's response to the UMIK1's known response.

To aggregate the data channels along the DAS microphone into a single data stream, we calculated an average strain rate for each cylinder according to

$$\dot{\epsilon}(t) = \frac{\dot{X}[t,x_2] - \dot{X}[t,x_1]}{|x_2 - x_1|}, \tag{1}$$

in which $\dot{\epsilon}(t)$ is the along-fiber strain rate (1/s); $\dot{X}$ is the along-fiber velocity (m/s, output format of interrogator unit); t is the time (s); and x_1 and x_2 are the start and end x positions of the fiber segment wrapping the cylinder. The physical meaning of the measurement is an averaged circumferential strain rate of the cylinder-fiber composite (assuming perfect fiber-cylinder coupling).

We compute a frequency-dependent signal-to-noise ratio, SNR(f), for each harmonic–microphone pair, which provides a means of comparing the frequency sensitivities between the DAS microphone and UMIK1. The SNR(f) is determined from the power spectrum composed of nonoverlapping short-time

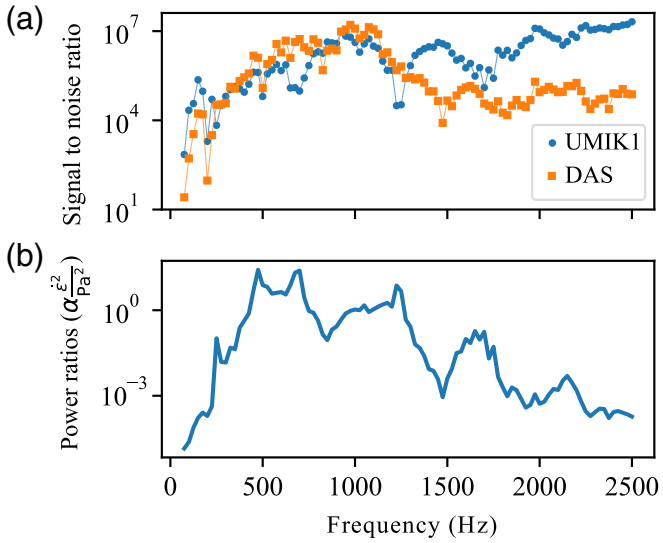

Figure 2. Distributed acoustic sensing (DAS)-microphone response showing (a) signal-to-noise ratios for the DAS microphone and UMIK1 measurement microphone for the tested harmonics, and (b) power ratio between DAS and UMIK1 microphones. The color version of this figure is available only in the electronic edition.

Fourier transform segments for 1.0 s of data for each microphone's recording of the harmonics and a quiet period taken as representative of background noise levels. We then divide the sum of the power spectra around the signal source frequency by the sum of the background noise over the same frequencies:

$$\mathrm{SNR}(f) = \frac{\sum_{f=f_1}^{f_2} S(f)}{\sum_{f=f_1}^{f_2} B(f)}, \tag{2}$$

in which $S(f)$ is the signal power spectrum; $B(f)$ is the background power spectrum; f is frequency (Hz); and frequency limits f_1 and f_2 are $f \pm 5$ Hz, respectively (Fig. 2a).

The power ratios between the microphones for each harmonic were calculated in a similar manner, but the output of the UMIK1 was first adjusted according to the amplitude calibration curve provided by the manufacturer:

$$P(f) = \frac{\sum_{f=f_1}^{f_2} P_{\mathrm{mic}}(f)}{\sum_{f=f_1}^{f_2} P'_{\mathrm{UMIK1}}(f)}, \tag{3}$$

in which $P_{\mathrm{mic}}(f)$ is the DAS-microphone power spectra; and $P'_{\mathrm{UMIK1}}(f)$ is the adjusted UMIK1 microphone power spectra (Fig. 2b).

Unfortunately, due to the complex interactions with various operating system-level features and settings, the sensitivity factor needed to convert P_{UMIK1} to absolute sound pressure level is scaled by some unknown constant (α). Moreover, the UMIK1 manufacturer provides no phase information for the microphone response. Therefore, Figure 2b shows a band-limited approximation of the power spectrum of the inverse of the transfer function scaled by α and cannot be used to convert from cylinder strain rate to absolute sound pressure level. However, Figure 2 is still useful in understanding general trends of the microphone response.

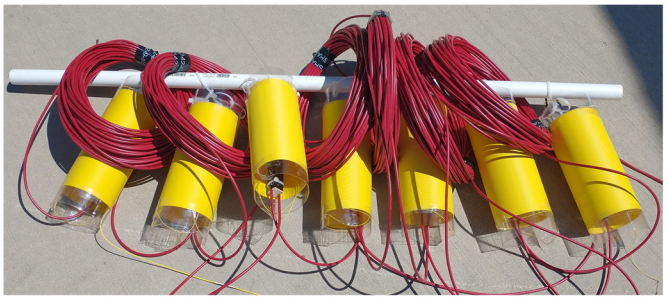

Figure 3. Microphone array. The lead cables (lose coils) connect the DAS microphones and are used to detect vibrations in the longwall. The microphones are composed of tight-buffered single-mode fiber wrapped around plastic (polyethylene terephthalate glycol) cylinders. The splice between lead cables and microphones is protected by a grooved block in the center of the cylinder. A chain of zip ties forms the cylinder handle and mounting point. The white pipe (top) is used for transportation. The color version of this figure is available only in the electronic edition.

Compared to the measurement microphones, the DAS cylinder microphone records lower SNR(f) values for most frequencies except for some bands between 500 and 1200 Hz. The DAS-microphone performance is probably acceptable over the entire tested range but, considering the sharp low-frequency drop-off in both plots of Figure 2, may not be adequate to record frequencies much lower than 75 Hz. The limited band response of the microphone is a major shortcoming, because the anticipated corner frequencies of mine events with moment magnitudes between 0 and 3 range from low hundreds to only a few Hz (Swanson *et al.*, 2016).

We also tested the effects of adding more cable between the interrogator and the microphone, which simulates longer cable runs and, because the microphones are just cable wrapped around plastic cylinders, more microphones in the array. We found that the background noise levels increased slightly, but there was no significant difference in the microphone response. Therefore, if the microphones are similar in their dimensions and length of wrapped cable, they will have very similar responses.

After characterizing the response of a single microphone, we developed an array of DAS microphones connected by signal cable (referred to as "lead cable") with a grooved block in the center of the cylinders to relieve tension and protect splices (Fig. 3). The entire array consisted of two sections each with seven DAS microphones.

ARRAY DEPLOYMENT

We conducted a field trial of our microphone array at an underground longwall coal mine in the western United

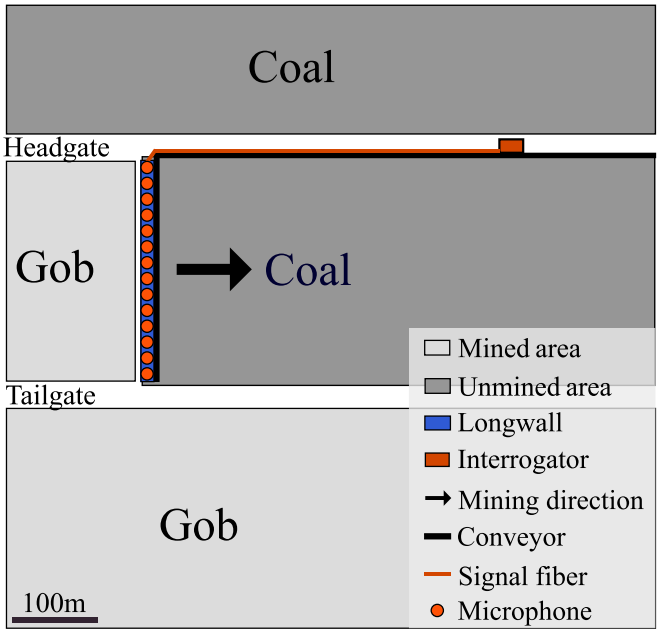

Figure 4. Map view of deployment and mining geometry. The gateroad pillars are omitted for simplicity. The color version of this figure is available only in the electronic edition.

States. The active panel was approximately 0.65 km deep. The interrogator was located at a power center (high-voltage transformer) approximately 0.4 km from the longwall. We fastened the fiber-optic signal cable to the monorail, which contains a suspended "accordion-like" structure that manages cables and hoses leading to the mining face by folding up as the longwall advances. The microphone array was connected to the signal cable, and one microphone deployed every ten shields—a span of approximately 17.2 m (Fig. 4). The lead cables were fastened to the longwall hydraulic hoses using zip ties. Because the hydraulic hoses must accommodate movement as shields advance, significantly more slack was needed than the width of a shield. Consequently, the length of the fiber-optic cable between each microphone was approximately 35 m. We performed a tap test to map each distance along the fiber to a physical location, and determined the distance ranges that constituted the microphones and lead cables. In addition, knowing the amount of fiber wrapped around the microphones and length of the lead cables provided bounds for these values. Although it is possible the cable fastened to the monorail recorded useful signals, it would be difficult to spatially orient the fiber because it gets folded up as the longwall advances. Consequently, we focused solely on the microphones and fiber deployed on the longwall.

The seismoacoustic array operated for 80 hr including three full 10 hr shifts and one partial shift. Around hour 80, one of the lead cables was pulled back into the gob, which disabled half of the array and ended data acquisition efforts. During the deployment, 35 seismic events were detected by a surface seismic network, ranging in magnitude from M_L 1.2 to 2.0. However, due to a small data gap, only 33 events were recorded by the DAS array. To manage the scope of this study, we restricted our efforts to examining signals from the 33 events; however, we are confident that the array could detect many more events, especially if the periodic noise associated with longwall operation can be suppressed with filtering.

PROCESSING METHODS

Data aggregation

The data associated with each microphone and lead cable sections were segmented, labeled, and stored based on the results of the tap test. Velocity data were then converted to strain rate for both types of fiber segments (DAS microphone and lead cables). First, the beginning and ending channels for each microphone were discarded to avoid contamination with lead cable data. Next, strain rates were calculated according to equation 1. For the microphones, x_1 and x_2 were selected to form a single channel for the entire microphone. For the lead cable, x_1 and x_2 span a single spatial channel (5.72 m). We retained only the center two channels for lead cables between each microphone. We then assigned a new distance to each strain-rate channel corresponding to center of the fiber's physical distance along the longwall face, 0 m being on the headgate side.

Waveform parameterization

Because full wavefield modeling is beyond the scope of this study, we selected two parameters to summarize the recorded signals. First, we manually inspected the lead cable channels for each event and estimated first arrival times. The microphone channels mostly exhibited emergent signals, and usually only a few (two to six) microphone recordings were significantly above the background noise levels. Although there are many approaches to quantifying signal amplitude, including peak values, duration, and statistical properties, we selected a modified form of standard deviation:

$$\sigma' = \sqrt{\frac{\sum(\dot{\epsilon}_s - \mu_l)^2}{N_s}}, \tag{4}$$

in which σ' is the modified standard deviation (strain/s); $\dot{\epsilon}_s$ is the short-time strain rate recorded by a given channel; μ_l is the long-time mean; and N_s is the number of samples in the short time window. The short time windows began at the first arrival time and lasted 1.0 s. We selected 1.0 s, because longer windows tended to dilute the short signals recorded by the lead cables (which typically had durations of about 0.25 s) and would occasionally capture nonevent-related strains from shields advancing. Shorter windows truncated significant portions of some microphone recordings. We selected a long time window of 60 s, because it greatly exceeded any observed signal duration. We did not perform any pre-filtering before calculating σ' and Table 1 provides the interrogator configuration.

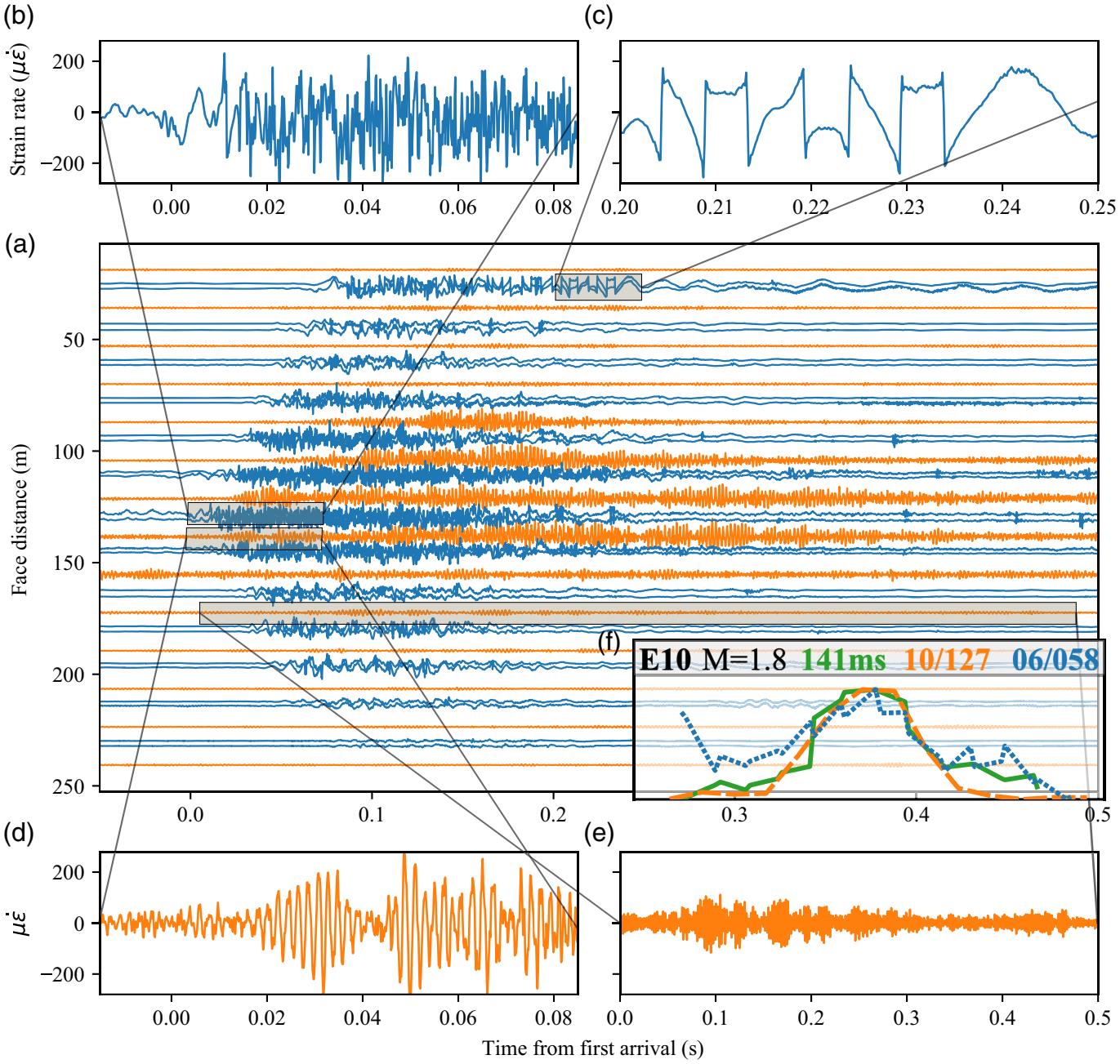

The long time window is used for calculating the mean, because some infrasound signals, particularly those associated with significant gas release such as volcanoes, can have large nonsymmetric impulses that would skew a short-term mean (McNutt *et al.*, 2015). Although it is unclear how well the DAS microphones might record such low-frequency signals, a longer time window should not adversely affect the measure. σ' is also desirable in that it accounts for both the initial pulse amplitudes (related to the seismic source for lead cables or air blast for microphones) and coda signals above the noise level (assumed to be interactions of ejected coal with the machinery and workings).

Figure 5. (a) Example of aggregated channels for event E10 showing a wiggle plot of microphone (single trace) and lead cable (double trace) channels normalized to the maximum value for each cable type and offset by face distance. (b,c) Also shown are zoomed-in waveforms for lead cable and (d,e) microphone channels. (f) The parameterization of the waveforms as shown in Figure 6 (note: *x* axis is face distance). See text in Results and Discussion sections for additional discussion. The color version of this figure is available only in the electronic edition.

RESULTS

Figure 5a shows waveforms of E10 with lead cable channels occurring in closely spaced pairs and microphone channels

spaced out. The lead cables generally record much higher frequencies near the first arrival and lower frequencies in later parts of the waveform. We observed some cycle-skipping in the lead cable channels (Fig. 5c), which occurs when the strain exceeds the setting-specific dynamic range of the interrogator. The cycle-skipping occurs later in the waveform and will certainly bias σ'_{lead}, which we discuss later. We did not observe any cycle-skipping in the microphone channels. The microphone recordings have emergent signals with well-pronounced harmonics around 500 Hz (Fig. 5d). The microphone signals drop off quickly with distance. For event E10, even 50 m from the first arriving lead cable channel, the microphone signal has nearly reached background levels (Fig. 5e).

Figure 6 shows the moveout and σ' for each event. All the 33 events are visible on both the microphones and the lead cable channels, despite high background noise levels during active mining. The lead cables show a clear moveout with the first arrival indicating the lateral location of the seismic event (see also Fig. 5). The first arrival picks made on the lead cable channels are generally smooth, but there are a few exceptions that have significant outliers or discontinuities (e.g., E23, E25, E30). The shapes of σ'_{mic} (red lines) are highly variable. Several events display narrow spikes near the first arrival (E02, E20, E31, E33), whereas others are almost Gaussian shaped (E03, E10, E12, E19, E28). The narrow spikes could indicate a smaller area at the face that experiences enough damage to generate significant acoustic energy in the workings. The sharp drop-off over distance is due to the rapid attenuation of the relatively high frequencies recorded by the DAS microphones and lack of new noise generated near the microphones that recorded a lower σ'_{mic}. Thus, high amplitudes of σ'_{mic} could correspond to face damage near the microphone, and sharp drop-offs could delineate the end of the damage zone. The observed σ'_{lead} values generally follow the same trends as σ'_{mic}, but they tend to be rougher and fall off less quickly as a function of face distance (e.g., E03, E04 E11, E20, E27). The apparent difference in propagation characteristics is due to the two segment types effectively recording two different propagation modes; the lead cables record seismic energy as it propagates through the longwall, whereas the microphones record the acoustic energy propagating in the workings.

Figure 7 shows the smoothed amplitude spectra recorded by both microphone and lead cable segments for the short time window used to calculate σ'. The colors show channels that recorded the maximum, the median, and the minimum values of σ' for each of the 33 events. The shaded regions delineate the first and the last decile, whereas the solid lines are the median of the frequency bins. Each microphone channel has a peak around 500 Hz (Fig. 7a), which corresponds to a spike in the frequency response (Fig. 2b). The microphone channels with the largest σ'_{mic} recorded significant energy in the lower frequency bands (compared to the other microphone channels), which indicates that the microphones can record low frequencies and that, perhaps, these low frequencies correspond to gas liberation associated with the damage at the face. The lead cable channel spectra show little variability (apart from being scaled up), but the slope of the maximum spectra is slightly steeper (Fig. 7b). The high frequencies in lead cable spectra may be artificially inflated by cycle-skipping (Fig. 5c).

Although we currently lack a full transfer function, it is informative to compare the strain-rate measurements recorded by the microphones in the lab and mine settings. Figure 8 shows the relationship between σ' (x axis) and the maximum absolute value of the short time window (y axis) for both types of recordings. For reference, the maximum values of $\max(\mu\dot{\epsilon})$ are 790 and 2620, and the maximum value of $\sigma(\mu\dot{\epsilon})$ are 180 and 1830 for coal burst recordings and lab recordings, respectively. Although the lab recordings have higher values in both metrics by up to an order of magnitude, this does not necessarily mean that the absolute sound pressure was higher in the lab but could simply be an artifact of the strong frequency response of the microphones. The lab recordings have a linear relationship between $\sigma(\mu\dot{\epsilon})$ and $\max(\mu\dot{\epsilon})$, because the signal is a simple sine wave.

DISCUSSION

Insights from monitoring

We now present a few observations about the nature of the events recorded by the seismoacoustic array. First, unsurprisingly, most of the events occur during active longwall mining, with only a single event occurring during an off-shift (Fig. 9a; E01). Because the moveout of E01 progresses roughly linearly from the tailgate to the headgate (Fig. 6), and the lead and microphone σ' values are low relative to the other events, E01 likely occurred in the adjacent mined-out panel. However, despite E01 inducing very little strain in the lead or microphone segments, it was still readily detectable in the absence of the mining noise.

Second, the events inducing the largest effect on the microphones, as measured by $\max(\sigma'_{\mathrm{mic}})$, were not the largest magnitude events. For example, the four events with the highest $\max(\sigma'_{\mathrm{mic}})$ values (Fig. 9, dashed outline; E06, E16, E20, and E24) had reported magnitude values of M_{L} 1.2, 1.4, 1.5, and 1.6, respectively. The four largest magnitude events (Fig. 9, dotted outline; E05, E09, E15, and E25) had average, or slightly above average $\max(\sigma'_{\mathrm{mic}})$ values but did have some of the largest $\max(\sigma'_{\mathrm{lead}})$ values, indicating that the seismic effect on the array was greater than the acoustic effect relative to other events. If the assertion expressed by several miners that louder events tend to cause more damage is correct, this provides evidence that event magnitude alone is insufficient for estimating surface damage. However, an alternative explanation is that the larger events' spectra were richer in lower frequencies and, because the microphone response drops off sharply (Fig. 2), the lower values of $\max(\sigma'_{\mathrm{mic}})$ for larger events might be an

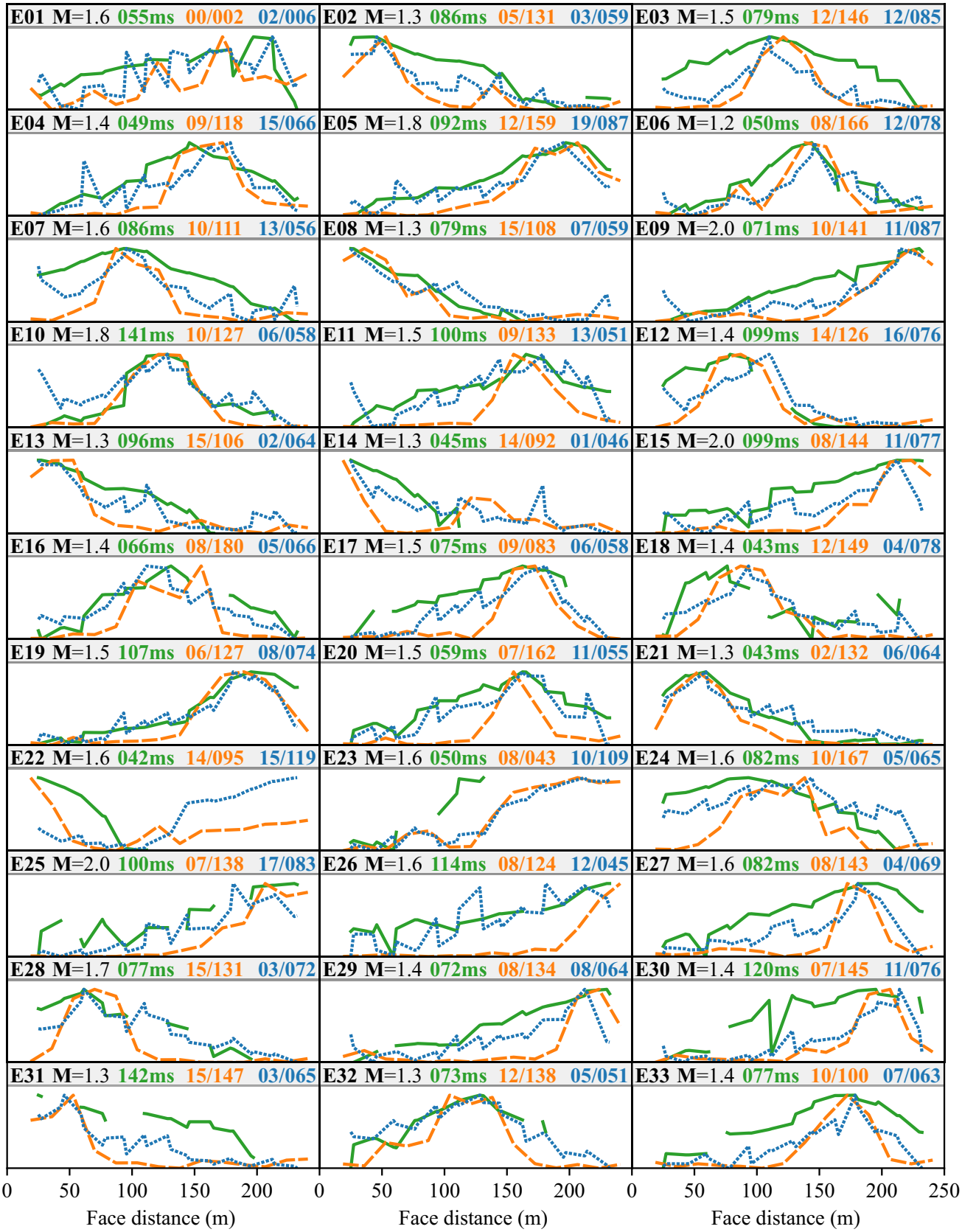

Figure 6. Moveout and modified standard deviation (σ') for the 33 events recorded by the DAS array and surface network. The text box above each plot shows first the event number, followed by the magnitude, moveout duration, and the minimum and the maximum σ' of strain rate for microphones channels and lead cable channels (in units of microstrain), respectively. The plots show the normalized moveout (solid line) with the first arrival at the top and the normalized modified standard deviation for each microphone channel (dashed line) and lead cable channel (dotted line) plotted as a function of face distance. The color version of this figure is available only in the electronic edition.

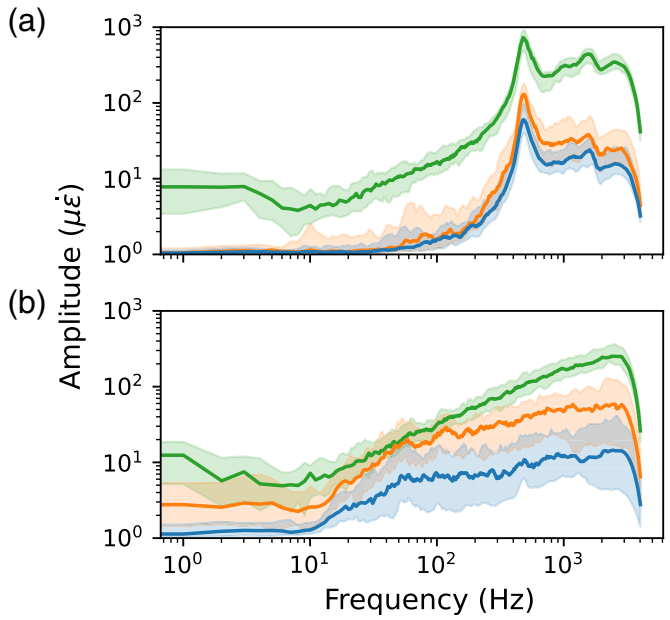

Figure 7. Smoothed spectra of event data recorded by (a) microphone channels and (b) lead cable channels for events with the largest (top), the median (middle), and the minimum (bottom) σ'. The shaded in regions delineate the bottom and top decile, whereas the solid lines show the median values. The color version of this figure is available only in the electronic edition.

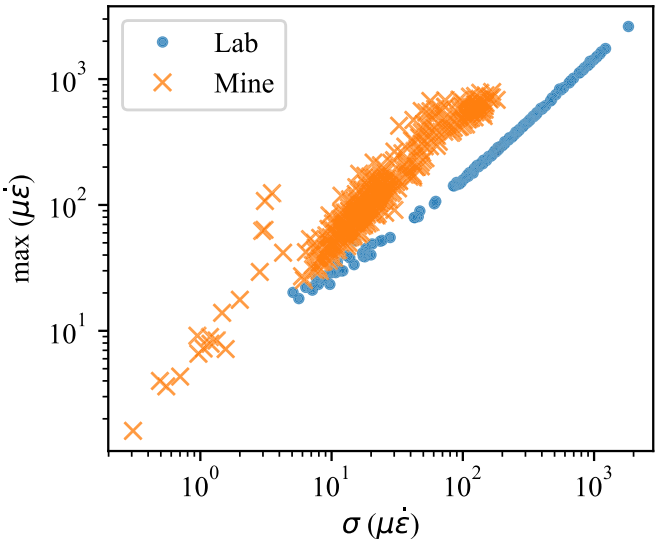

Figure 8. Comparison of DAS-microphone statistics for harmonics recorded in the lab (dots) and in-mine event recordings (x's) for max strain (y axis) and mean strain (x axis). The color version of this figure is available only in the electronic edition.

artifact of the microphone response. Events E01, E22, and E23 are unique, because their max(σ'_{lead}) values are greater than their max(σ'_{mic}) values. Examining their moveouts and relative face positions (Figs. 6 and 9c) suggests that this could be due to the events occurring off the panel. In addition, for both E22

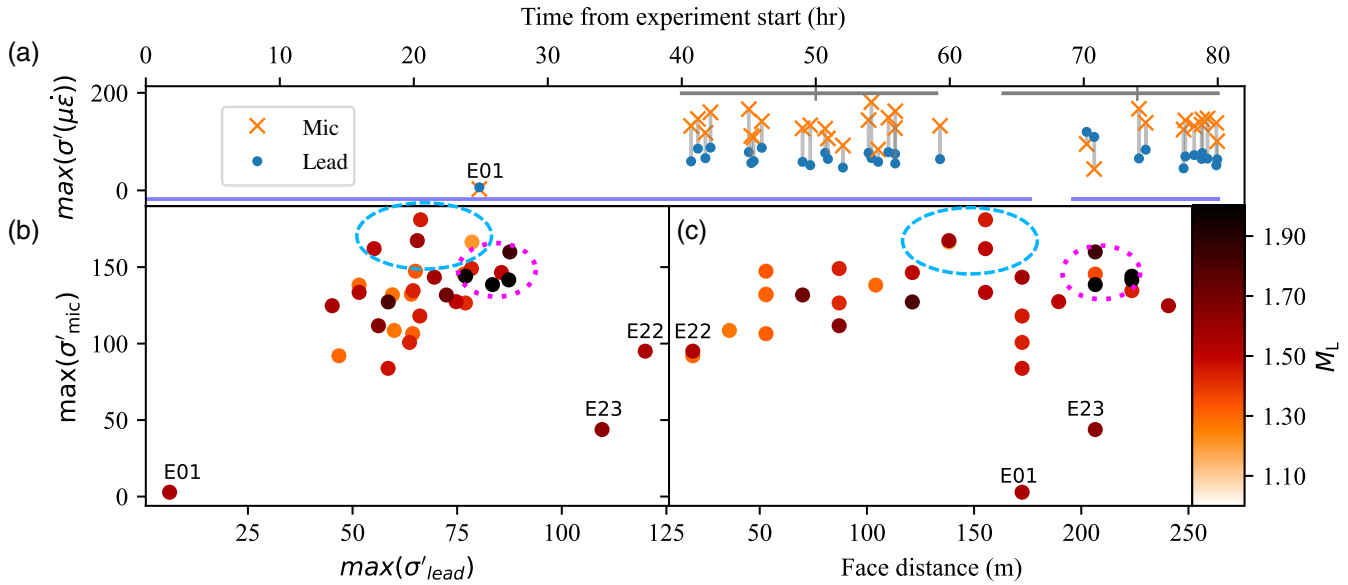

Figure 9. The maximum standard deviation of strain rate for microphone segments (max(σ'_{mic})) and lead cable segments (max(σ'_{lead})). (a) max(σ'_{mic}) (x's) and max(σ'_{lead}) (dots) as a function of experiment duration for each event. The horizontal lines near the top of the panel indicate active longwall mining times, and the horizontal line toward the bottom indicates data availability. (b) max(σ'_{lead}) (x axis) versus max(σ'_{mic}) (y axis) colored by magnitude. (c) max(σ'_{mic}) plotted against face distance shaded by event magnitude. All strain-rate values are reported in microstrain. The dashed blue outline in panels (b) and (c) encompasses the four events (two dots are colocated in panel (c) with the highest max(σ'_{mic}), and the dashed pink outline encompasses the four highest magnitude events. The color version of this figure is available only in the electronic edition.

and E23, noise levels appear elevated for channels on the tailgate side of the panel, which could be caused by a temporary pinching of the lead cable (see Data and Resources).

Given that local magnitude is based on logarithmic measurements of far-field waveform amplitudes, the fact that σ' increases relatively little for both cable types may seem odd. For example, most events have $\max(\sigma'_{\mathrm{mic}})$ values between 150 and 200 $\mu\epsilon$ and $\max(\sigma'_{\mathrm{lead}})$ between 40 and 100 $\mu\epsilon$ despite a spread of nearly 1 local magnitude. This could be due to several factors. First, the relation between the source spectra and the signals recorded by the DAS array is certainly complex, considering the wavefield interactions between the mine openings and equipment and the strong frequency response of the sensors. Second, cycle-skipping introduces by bias by reducing (σ'_{lead}). Finally, because the recordings are taken so close to the sources, there are certainly near-field effects that could complicate the relationship.

Finally, the location of the microphone that recorded $\max(\sigma'_{\mathrm{mic}})$ has a possible geomechanical interpretation. First, the maximum confinement of the coal, or more precisely the maximum of the first invariant of the stress tensor, occurs in the center of the panel. This means greater energy release per failed volume, and that the least resistance for the expanding volume is in the direction of the mining face when the coal rapidly dilates. Therefore, with all else being equal (including source dimension), events occurring in the center of the panel will tend to release more energy than events in other locations. Second, there are significant abutment loads from the adjacent mined-out panel that are maximized on the tailgate side of the current panel. However, because there is less confinement on the tailgate side, peak strengths are lower, and more of the strain-burst volume can expand to the tailgate, causing less damage to the longwall face even for higher magnitude events. Therefore, the trade-off between higher stresses on the tailgate and higher confinement in the center of the panel could explain why the events with the highest $\max(\sigma'_{\mathrm{mic}})$ are located between the center of the panel and the tailgate.

DAS potential for coal mine seismic monitoring

The DAS-based monitoring approach we present provides several advantages over conventional in-mine monitoring. First, it alleviates the significant burden of frequently moving sensors. For our configuration, only the interrogator would need to be moved each time the power center is advanced, and the DAS cable would be relocated with the power cables. However, because this is only a small step in an otherwise standard activity, the additional burden on mine personnel would be minimal. Second, unlike other monitoring systems with conventional electronics, DAS exclusively uses light transmission, and there are no permissibility restraints, given the interrogator is located in fresh air, because it can employ MSHA-approved fiber-optic cable. Third, this system provides a measurement of energy release near the source and the workers. Although further study is needed, these measurements may be better able to quantify risk and damage than traditional seismic recordings, which is a topic we discuss in the next section. In short, our method may be more pragmatic for mines concerned about coal bursts near the longwall face than current monitoring approaches.

Of course, the system does have some disadvantages. First, due to the complex interactions between the mining equipment, ground, and cable, the fact that many of the recordings are probably not taken in the far field, and the lack of DAS broadside sensitivity (Hornman, 2017), it would be extremely difficult to quantitatively relate recorded measurements back to particle motion in the rock—a necessity to estimate many of the conventional seismic source parameters. Second, because the system is colocated with mining activity, the background noise levels are extremely high, undoubtedly degrading the system's ability to detect small events. However, given the recent advances in machine learning denoising techniques (e.g., Yu *et al.*, 2019), and because the noise sources are relatively periodic, adaptive filtering may prove effective for mitigating this shortcoming. Third, the longwall is a very harsh environment, so future arrays will need to be made very robust and carefully deployed to survive.

A hybrid monitoring strategy could combine both conventional monitoring and the longwall-based DAS approach presented in this article. Such a network could include a sparse geophone array located on the mine surface or throughout the mine, which would not require frequent relocation and could be placed in fresh air. The geophone network could then be used to calculate source parameters and constrain event locations outside of the current panel. The longwall DAS system would provide kinematic information for travel-time-based locations and an acoustic measure of damage for events occurring on the mining face. Of course, the two systems would need to be time synchronized and the position of the longwall recorded with fine temporal resolution as it advances.

Moreover, several studies have recognized that rapid gas desorption can contribute significant energy to coal bursts (e.g., Zhou *et al.*, 2018; Cao *et al.*, 2019). Pressure readings taken close to the damage area may help better quantify the role gas release plays for specific coal bursts and lead to a better understanding of coal burst mechanisms, and thus inform mitigation measures. Indeed, the low frequencies (<30 Hz) detected by some of the DAS microphones may be due to gas liberation associated with the coal burst process (Fig. 7a).

DAS-seismoacoustic damage monitoring

Current seismic monitoring methods produce a discrete catalog of seismic event source parameters and sparse recordings of ground motion at each sensor. However, complexities such as location errors, site characteristics, performance of installed ground support, local stress perturbations, triggering of secondary sources, and many other factors, all complicate the

relationship between source parameters and observed damage. For example, Hudyma *et al.* (2016) found that for a Canadian hardrock mine, the magnitude–damage relationship was "crude" with widely varying volumes of ejected material for a given magnitude. Heal (2010) performed a comprehensive study of about 250 rockbursts and found that, in addition to location and magnitude, local stress information, ground support capacity, peak particle velocity, local geological information, and several other factors were required to explain roughly 80% of the observed variation in a qualitative damage rating. The difficulty in relating the outputs of seismic monitoring (source parameters) to mine damage motivated Potvin (2017) to highlight the need for advancements in estimating risk and dynamic support demands, partially because "measurements in the near field of significant seismic events are very difficult to achieve."

DAS-based monitoring approaches, due to their highly distributed nature and the cost-effectiveness of fiber-optic cable, may be able to provide the near-field measurements needed to better estimate support demands and quantify damage severity. In this regard, we have demonstrated DAS-based near-field measurements in an underground coal mine, and that both seismic and acoustic measurements may be useful in this endeavor. Our approach, however, is not limited to longwall coal mining. A single DAS interrogator could support hundreds of seismic or acoustic monitoring channels distributed throughout any underground environment. If many sensors are deployed, particularly in high-risk areas, the system could capture a significant number of near-damage recordings.

Future work

The DAS microphones have a sharp drop-off for lower frequencies (Fig. 2), but including a closed volume in the design could drastically improve the low-frequency response. For example, one might consider inserting and inflating a balloon in the center of the cylinder, which would expand or contract in response to quasi-static (low-frequency) changes in air pressure. The expansion or contraction would then be translated to radial strain on the cylinder and recorded by the DAS system. Wooler and Crickmore (2007) employed this principle in their DAS-based microphones that recorded low frequencies related to gun shots. In addition, more rigorous acoustic testing (including lower frequencies) and microphone response quantification are needed to develop a broadband transfer function to convert between measured strain and air pressure for the DAS-based microphone.

A more robust cable and microphone design will be needed for the system to survive in the rugged longwall environment. A more thorough fastening of the lead cables to the longwall could have perhaps prevented the failure our array experienced; however, higher rated fiber-optic cable would also be prudent to resist the frequent abrasion of moving parts and potential rock impacts. Smaller, hardened microphones that could be deployed more densely would also improve the array's usability and longevity.

Although no interpretation or data processing advances are needed to use the first arrivals to better constrain event locations, more research to relate damage at rock surfaces to the signals recorded by the seismoacoustic array would greatly amplify the usefulness of the array data to improve seismic risk management. Furthering the study of mine damage acoustics will require significant theoretical, numerical, and observational advances.

Cycle-skipping issues need to be addressed either through more advanced phase-unwrapping algorithms, using different waveforms measurements that are insensitive to cycle-skipping (e.g., signal duration), or perhaps extracting the standard deviation from a temporal derivative of strain rate after despiking.

CONCLUSIONS

Here, we present a DAS-based monitoring strategy that effectively turns an active longwall into a seismoacoustic array, thereby alleviating many of the shortcomings related to traditional in-mine burst monitoring. We demonstrate that the array can record both seismic and acoustic signals of mining-induced seismicity. We find that a modified standard deviation of the recordings, although the lead cable measures are biased by cycle-skipping, may be beneficial for understanding coal burst-related damage. This type of array is potentially useful for understanding damage related to dynamic failures in other mining contexts as well. However, significant work remains to improve microphone design, data interpretation and processing, and array robustness.

DATA AND RESOURCES

Data used in this study were collected in the manner described in the previous sections. They are considered proprietary as part of the collaborative agreement between the National Institute for Occupational Safety and Health (NIOSH) and the unnamed coal mine. However, the supplemental material, including several recordings from the distributed acoustic sensing (DAS) microphones and waveform plots of all the 33 events, may be found at https://derchambers.com/publications/bssa-2023 (last accessed March 2023).

DECLARATION OF COMPETING INTERESTS

The authors declare no competing interests.

ACKNOWLEDGMENTS

The authors would like to thank:

- the engineering staff at the collaborating coal mine for facilitating the array deployment;
- Michael Roelens and the other Terra15 staff who provided excellent support in helping us troubleshoot issues and improve our experiment;
- Duncan Marriott of Chaparral Geophysics for insightful conversations about acoustic monitoring and microphone design;

- Gabe Walton, Shawn Boltz, Peter Swanson, and two anonymous reviewers for providing insights and comments to improve this work;
- Allen Chambers for lending his shop and expertise to construct the seismoacoustic array;
- and Jim Garner and Will Ray of Oak Ridge National Lab for providing some of the fiber optic cable.

The findings and conclusions in this report are those of the author(s) and do not necessarily represent the official position of the National Institute for Occupational Safety and Health (NIOSH), Centers for Disease Control and Prevention (CDC). Mention of any company or product does not constitute endorsement by NIOSH, CDC.

REFERENCES

Bucaro, J. A., N. Lagakos, B. H. Houston, J. Jarzynski, and M. Zalalutdinov (2005). Miniature, high performance, low-cost fiber optic microphone, *J. Acoust. Soc. Am.* **118**, 1406–1413.

Cao, J., H. Sun, B. Wang, L. Dai, B. Zhao, G. Wen, and X. Zhao (2019). A novel large-scale three-dimensional apparatus to study mechanisms of coal and gas outburst, *Int. J. Rock Mech. Min. Sci.* **118,** 52–62.

Cole, J. H., R. L. Johnson, and P. G. Bhuta (1977). Fiber-optic detection of sound, *J. Acoust. Soc. Am.* **62,** 1136–1138.

Du Toit, H. J., G. Goldswain, and O. Gerrit (2022). Can DAS be used to monitor mining induced seismicity? *Int. J. Rock Mech. Min. Sci.* **155,** 105127.

Heal, D. (2010). Observations and analysis of incidences of rockburst damage in underground mines, *Ph.D. Thesis*, The University of Western Australia, Perth, Australia.

Hornman, J. C. (2017). Field trial of seismic recording using distributed acoustic sensing with broadside sensitive fibre-optic cables, *Geophys. Prospect.* **65,** 35–46.

Hudyma, M., L. Brown, and D. Cortolezzis (2016). Seismic risk in Canadian mines, CIM MEMO, available at https://www.researchgate.net/profile/Marty-Hudyma/publication/309176397_Seismic_Risk_in_Canadian_Mines/links/5803b9c708ae310e0d9f4e73/Seismic-Risk-in-Canadian-Mines.pdf (last accessed March 2023).

Karacan, C. Ö. (2008). Modeling and prediction of ventilation methane emissions of US longwall mines using supervised artificial neural networks, *Int. J. Coal Geol.* **73,** 371–387.

Li, H., Q. Sun, T. Liu, C. Fan, T. He, Z. Yan, D. Liu, and P. P. Shum (2020). Ultra-high sensitive quasi-distributed acoustic sensor based on coherent OTDR and cylindrical transducer, *J. Lightwave Tech.* **38,** 929–938.

Lindsey, N. J., and E. R. Martin (2021). Fiber-optic seismology, *Annu. Rev. Earth Planet. Sci.* **49,** 309–336.

Lior, I., E. D. Mercerat, D. Rivet, A. Sladen, and J. P. Ampuero (2021). Imaging an underwater basin and its resonance modes using optical fiber distributed acoustic sensing, *Seismol. Res. Lett.* **93,** 1573–1584.

Liu, Z., L. Zhang, H. Wei, Z. Xiao, Z. Qiu, R. Sun, F. Pang, and T. Wang (2021). Underwater acoustic source localization based on phase-sensitive optical time domain reflectometry, *Opt. Express* **29,** 12,880–12,892.

Luo, X., and Y. Duan (2022). Microseismic monitoring of longwall caving process using distributed optic fiber sensing, *55th US Rock Mechanics/Geomechanics Symposium*, 20–23 June 2021, Paper Number 1359.

Mark, C. (2016). Coal bursts in the deep longwall mines of the United States, *Int. J. Coal Sci. Tech.* **3,** 1–9.

Mark, C. (2018). Coal bursts that occur during development: A rock mechanics enigma, *Int. J. Min. Sci. Tecnol.* **28,** 35–42.

McNutt, S. R., G. Thompson, J. Johnson, S. De Angelis, and D. Fee (2015). Seismic and infrasonic monitoring, in *The Encyclopedia of Volcanoes (Second Edition)*, H. Sigurdsson (Editor), Academic Press, Amsterdam, 1071–1099.

Mendecki, A. J., R. A. Lynch, and D. A. Malovichko (2010). Routine micro-seismic monitoring in mines, *AEES Annu. Conf.*, Perth, Australia, 1–33.

Mutke, G., J. Dubiński, and A. Lurka (2015). New criteria to assess seismic and rock burst hazard in coal mines, *Arch. Min. Sci.* **60,** 743–760.

Potvin, Y. (2017). The need for new technology to optimise the engineering design of ground support systems in underground mines, *Proc. First Int. Conf. Underground Min. Tec.*, Australian Centre for Geomechanics, 9–22.

Qi, Q., J. Li, Y. Ning, Z. Ouyang, S. Zhao, and L. Wei (2015). The technology and practice of rockburst prevention in Chinese deep coal mines, *49th US Rock Mechanics/Geomechanics Symposium*, Paper Number 849.

Rong, H., N. Li, H. Zhang, D. Sun, and B. Huo (2022). Insights into fundamental problems of rockburst under the modern structure stress field, *Sci. Reports* **12,** 1–11.

Swanson, P., M. S. Boltz, and D. Chambers (2016). Seismic monitoring strategies for deep longwall coal mines, *National Institute for Occupational Safety and Health Tech. Rept. 1944.*

Wooler, J. P., and R. I. Crickmore (2007). Fiber-optic microphones for battlefield acoustics, *Appl. Opt.* **46,** 2486–2491.

Yu, S., J. Ma, and W. Wang (2019). Deep learning for denoising, *Geophysics* **84,** V333–V350.

Zeng, X., H. F. Wang, N. Lord, D. Fratta, and T. Coleman (2021). Field trial of distributed acoustic sensing in an active room-and-pillar mine, in *Distributed Acoustic Sensing in Geophysics: Methods and Applications*, Y. Li, M. Karrenbach, and J. B. Ajo-Franklin (Editors), Wiley, Hoboken, New Jersey, 65–79.

Zhou, A., K. Wang, T. Feng, J. Wang, and W. Zhao (2018). Effects of fast-desorbed gas on the propagation characteristics of outburst shock waves and gas flows in underground roadways, *Process Saf. Environ. Protect.* **119,** 295–303.

Zuo, M., X. Tu, S. Yang, H. Fang, X. Wen, and F. Qu (2021). Channel distribution and noise characteristics of distributed acoustic sensing underwater communications, *IEEE Sens. J.* **21,** 24,185–24,194.

Manuscript received 1 November 2022
Published online 10 April 2023